Available online at www.sciencedirect.com
SCIENCE DIRECT®
Journal of Nuclear Materials 324 (2004) 33–40
journal of nuclear materials
www.elsevier.com/locate/jnucmat

Effect of microstructure on the cleavage fracture strength of low carbon Mn–Ni–Mo bainitic steels

Young-Roc Im [a], Byeong-Joo Lee [b], Yong Jun Oh [c], Jun Hwa Hong [d], Hu-Chul Lee [a,*]

[a] School of Materials Science and Engineering, Seoul National University, Shinrim-dong San 56-1, Kwanak-ku, Seoul 151-742, South Korea
[b] Department of Materials Science and Engineering, Pohang University of Science and Technology, Pohang 790-784, South Korea
[c] Advanced Materials Engineering Division, Hanbat National University, Taejon 305-719, South Korea
[d] Korea Atomic Energy Research Institute, Taejon 305-353, South Korea

Received 28 October 2002; accepted 6 September 2003

Abstract

The effects of the microstructure on the cleavage fracture strength of low carbon Mn–Ni–Mo bainitic steels were examined. A four-point bend test and double-notched bend specimens were used to measure the cleavage fracture strength of the alloys and identify the cleavage initiating micro-cracks, respectively. The cleavage fracture strength and DBTT of Mn–Ni–Mo bainitic steels were strongly affected by the alloy carbon content. The decrease in the alloy carbon content resulted in a decrease in the inter-lath cementite-crowded layers and higher cleavage fracture strength. Micro-cracks that formed across the inter-lath cementite-crowded layers were observed to initiate cleavage fracture. The width of these inter-lath cementite-crowded layers was accepted as a cleavage initiating micro-crack size in the micro-mechanical modeling of the cleavage fracture, and the measured cleavage strength values of the bainitic Mn–Ni–Mo steels were well represented by the modified Griffith relationship.

PACS: 81.70.Bt; 81.40.Np

1. Introduction

Nuclear pressure vessels are continuously exposed to neutron irradiation during their service, and this neutron irradiation raises the ductile to brittle transition temperature (DBTT) of pressure vessel materials. A lower DBTT as possible is one of the prime design goals for nuclear structural steels. The ductile to brittle transition of a BCC material is associated with the change in the fracture mode from void coalescence to cleavage fracture as a result of competition between the yield strength and the cleavage strength. The DBTT of the alloy can be lowered by raising the cleavage strength. It is well recognized that cleavage fracture in low alloy steels occurs when existing micro-cracks propagate through the ferrite matrix by an applied tensile stress. Various types of micro-mechanical models for cleavage fracture have been suggested [1–9]. The existing micro-crack size is dependent on the microstructure of the alloys. Grain boundary carbides [7,10–12], carbides in the ferrite matrix [13–18], non-metallic inclusions [19,20] or the grain/packet size [21–25] are often reported as the microstructural features that initiate cleavage fracture.

The cleavage fracture strength can be related to the existing micro-cracks through a modified Griffith [1] type equation:

$$\sigma_f = [4E\gamma_p/\pi(1-\nu^2)a]^{1/2},$$

* Corresponding author.
E-mail address: huchul@plaza.snu.ac.kr (H.-C. Lee).

0022-3115/$ - see front matter © 2003 Elsevier B.V. All rights reserved.
doi:10.1016/j.jnucmat.2003.09.003

where a is the size of the micro-crack that initiates the cleavage fracture, γ_p the effective surface energy, E the Young's modulus and v is the Poisson's ratio of the alloy. To improve the DBTT of an alloy, the microstructural parameters that control the size of the microcracks are controlled by the alloy chemistry and processing. In this work, the cleavage fracture strength of low carbon Mn–Ni–Mo bainitic alloys was measured and the microstructural parameters controlling the cleavage fracture of these alloys were identified. The cleavage fracture strength of the alloys was related to the width of the cementite-crowded inter-lath layer via the modified Griffith relationship.

2. Experimental procedure

2.1. Materials and heat treatments

The chemical composition of the Mn–Ni–Mo steels investigated in this study is listed in Table 1 with the ASME specifications for SA508 cl.3 steel. A laboratory alloy composition of typical SA508 cl.3 steel was also prepared as the reference alloy (labeled as 'S'). Many of the experimental alloys have lower carbon or higher Mo contents than the reference alloy. This study aimed to reduce the volume fraction of the cementite phase by decreasing the carbon content and/or by transforming it to a M_2C type carbides by increasing the Mo content in the alloys. In this study, the total amounts of the substitutional alloying elements, Mn and Ni, or Mo, were increased in order to compensate for the probable decrease in the hardenability in association with the decrease in the carbon content.

The thermo-mechanical processing schedule of the experimental alloys was arranged to duplicate the actual manufacturing conditions of the quench-and-tempered nuclear pressure vessel. The austenitizing conditions were controlled to produce a prior austenite grain size of approximately 30 μm in order to minimize the grain size effects on the mechanical properties of these steels. The cooling rate from the austenitizing temperature was selected in accordance with the reported value of 20 °C/min, as measured from the 1/4t thickness position of the pressure vessel. The tempering treatment was conducted at 660 °C for 10 h.

2.2. Mechanical testing

The cleavage fracture strengths of the alloys were evaluated by a four-point bend test at low temperatures, mainly at the liquid nitrogen temperature, using an Instron type tensile testing machine with a 15 ton capacity. The geometry of the four-point bend specimen is shown in Fig. 1(a). Cleavage fracture strength of the specimen was calculated as follows using the result of finite element analysis reported by Griffiths and Owen [26]. Their FEM calculation gives the stress intensification, $R = \sigma_{1\max}/\sigma_y$, as a function of the ratio of nominal bending stress to yield strength, $\sigma_{\text{nom}}/\sigma_y$, where $\sigma_{1\max}$ and σ_{nom}

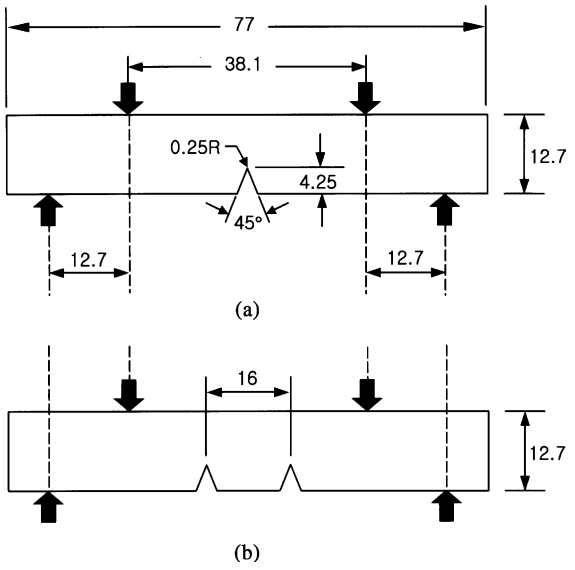

Fig. 1. Geometries of the four-point bend specimens (dimensions in mm): (a) single-notched specimen; (b) double-notched specimen for the cleavage nuclei observation.

Table 1
Chemical composition of the tested alloys (wt%)

Alloy	C	Mn	Ni	Mo	Cr	Si	Al
SA508 III	0.25	1.20	0.40	0.45	0.25	0.15	–
(ASME)	max.	~1.50	~1.00	~0.60	max.	~0.40	–
S	0.20	1.37	0.91	0.48	0.15	0.21	0.030
A	0.20	0.68	1.88	0.50	0.15	0.20	0.030
B	0.15	0.99	1.90	0.60	0.15	0.19	0.031
C	0.16	1.01	1.48	0.49	0.15	0.21	0.021
D	0.10	0.70	1.48	0.76	0.15	0.21	0.023

represent the maximum tensile stress below the notch and the nominal bending stress, respectively. σ_y is the yield stress of the alloy measured by tensile test. Nominal bending stress σ_{nom} was calculated from the applied maximum load, P, in four-point bend test by the relation $\sigma_{nom} = 3P/a^2$, where a is the specimen depth below the notch. The $\sigma_{1\,max}$ value obtained by multiplying stress intensification, R, to yield strength of the alloy was accepted as the alloy cleavage fracture strength.

Double-notched bend specimens of the geometry shown in Fig. 1(b) were also used to identify the cleavage crack nuclei after loading to failure. In the four-point bend test, the bending moment between the two upper loading anvils is constant to develop equivalent stress state at the tips of the both notches. One of the notches in the more vulnerable micro-mechanical condition will be fractured, and the unbroken ligament below the remaining notch reveals the micro-mechanical states just prior to fracture. After loading to fracture, the unbroken notches were sectioned as shown in Fig. 2 and the development of micro-cracks under the unbroken notches were observed using SEM after etching the sectioned unbroken ligament.

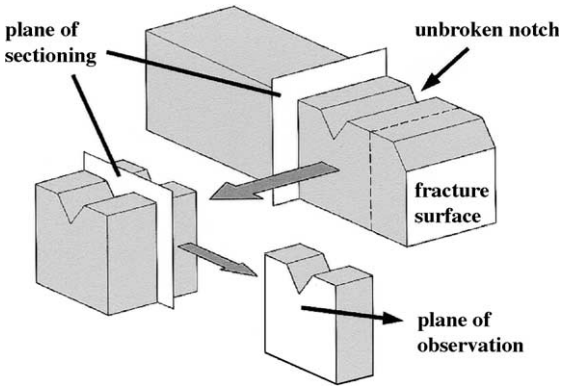

Fig. 2. Sectioning of unbroken ligament of double-notched specimen for the observation of the nuclei for cleavage fracture.

2.3. Microstructural investigation

Microstructure of the tempered alloys was observed by optical and scanning electron microscopy. Metallographic specimens were prepared by grinding and final polishing to 0.3 μm alumina polishing powder. The specimens were then etched in 2% Nital or a 1:1 mixed solution of Nital and Picral. A carbon extraction replica technique was employed to investigate the overall distribution of carbides and to analyze individual carbide particles in detail. Carbon extraction replicas and conventional thin foil specimens were examined using JEM 200CX transmission electron microscope (TEM).

The width of the inter-lath cementite-crowded area, which is accepted as the microstructural unit for cleavage fracture nucleation, was measured from the SEM images obtained by JSM-5600 scanning electron microscope. Nearly 200 data points were measured and 95th percentile largest size was accepted as the size of the microstructural unit. This microstructural unit was used in the micro-mechanical modeling of the cleavage fracture strength.

3. Results

3.1. Microstructure of Mn–Ni–Mo bainitic alloys

Typical microstructural features of the reference alloy 'S' are shown in Fig. 3. The figure shows the tempered upper bainitic structure with cementite-crowded regions (arrowed in Fig. 3(a) and (b)) between the bainitic ferrite laths. This inter-lath region formed in the later stages of the bainite transformation and is populated with long rod type (about 0.3 μm thick and 3 μm long) and spherical type (about 0.3 μm in size) cementite particles. Densely distributed fine needle like M_2C

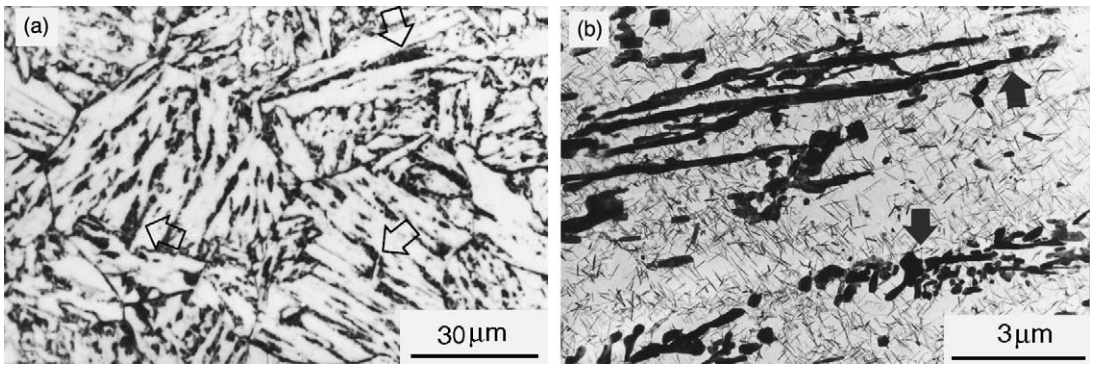

Fig. 3. Tempered upper bainitic microstructure of the reference alloy 'S': (a) optical micrograph; (b) TEM micrograph (replica).

Table 2
Calculated weight fraction of cementite and the M_2C carbides at the tempering temperature

Alloy	Precipitates (wt%, 650 °C)	
	M_2C	Cementite
S	0.33	2.61
A	0.34	2.56
B	0.48	1.83
C	0.34	1.92
D	0.67	0.79

carbides (about 0.02 μm thick and 0.3 μm long) were observed within the ferrite laths (Fig. 3(b)), which precipitated mainly during the tempering treatment.

The equilibrium fraction of the carbides in the experimental alloys at the tempering temperature, 660 °C, was calculated and is listed in Table 2. The details of the calculation and the reliability of the calculation based on the CALPHAD method in these types of steels are reported elsewhere [27,28]. Thermodynamic calculations show that the volume fraction of the cementite, which was identified as the main fracture source in this type of steel [28], can be reduced by decreasing the carbon content and/or by increasing the Mo concentration of the alloys. The optical micrographs presented in Fig. 4 show that the area fraction and width of the inter-lath cementite-crowded areas decrease with decreasing alloy carbon content. The 95th percentile and average width of the inter-lath layers were measured and are listed in Table 3. Fig. 5 shows that the 95th percentile width of the inter-lath layers decreases linearly with decreasing cementite volume fraction of the alloys.

3.2. Cleavage fracture strength of Mn–Ni–Mo bainitic alloys

3.2.1. Temperature dependence of cleavage fracture strength

The cleavage fracture strengths of alloy 'S' measured at different temperatures by the four-point bend test are shown in Fig. 6. Alloy 'S' has an almost identical cleavage fracture strength of approximately 1670 MPa at temperatures of −196, −150, and −135 °C. The cleavage fracture strength of the low carbon steels can be explained either by the propagation control model or by the nucleation control model. In the nucleation control model [2–4], crack formation is believed to be the controlling stage for the cleavage fracture. The stress to propagate the nucleated crack is lower than the stress to form the crack nuclei. In the propagation model [1,7–9], the pre-existence of crack nuclei is assumed and cleavage

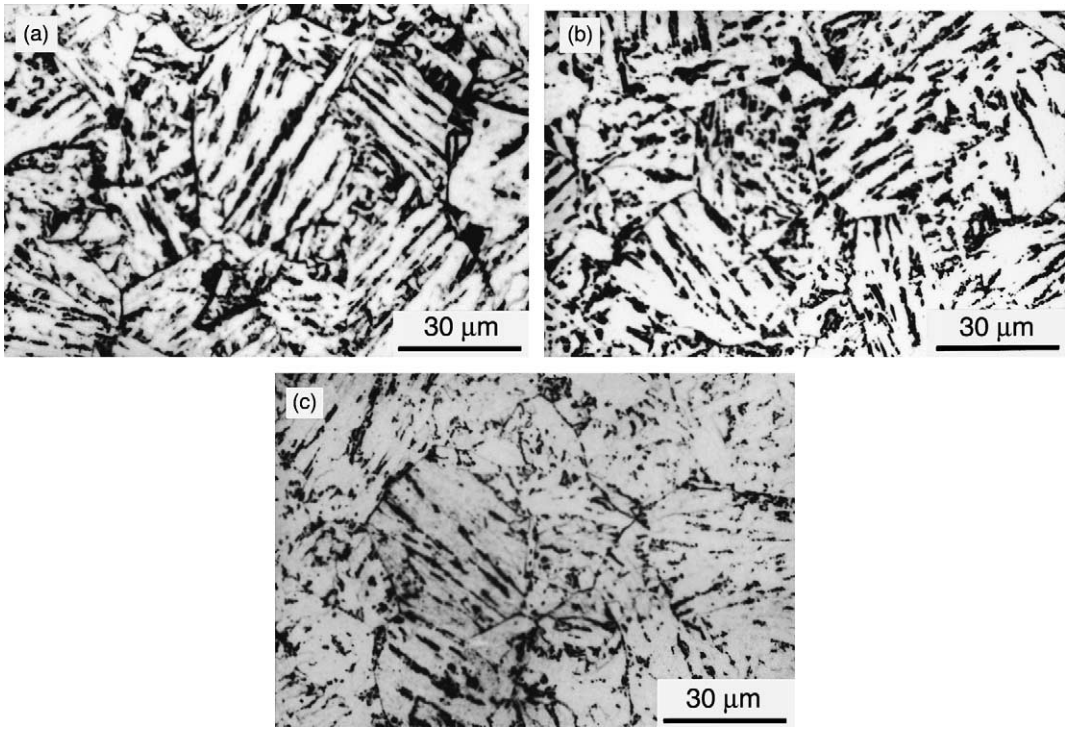

Fig. 4. Optical and scanning electron micrographs of the tested alloys: (a) 0.20 wt% C and 0.5 wt% Mo alloy 'A'; (b) 0.15 wt% C and 0.5 wt% Mo alloy 'C'; (c) 0.10 wt% C and 0.8 wt% Mo alloy 'D'.

Table 3
Average and 95th percentile sizes of the microstructural units

	Microstructural unit	S	A	B	C	D
95th% size (μm)	Inter-lath layer (width)	2.92	2.92	2.69	2.48	2.04
	Cementite (thickness)	0.44	0.42	0.49	0.46	0.49
Average size (μm)	Inter-lath layer (width)	1.77	1.77	1.62	1.63	1.27
	Cementite (thickness)	0.33	0.31	0.36	0.34	0.33

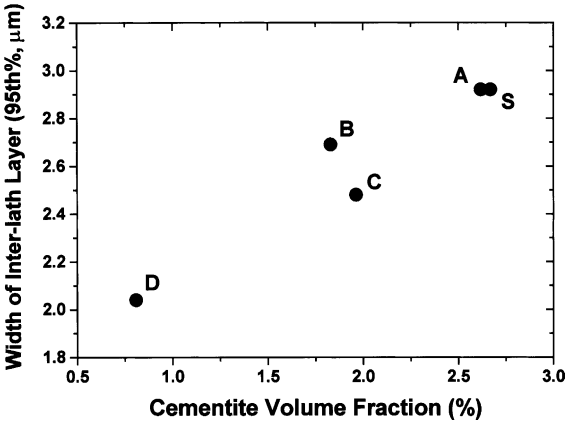

Fig. 5. The relation between the calculated cementite volume fractions and the measured 95th percentile width of the cementite-crowded inter-lath layer.

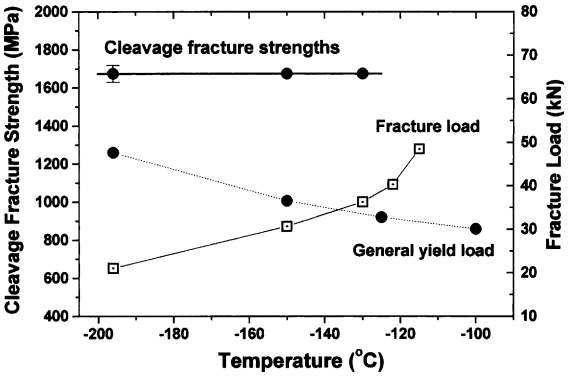

Fig. 6. Temperature independency of the cleavage strength of alloy 'S'.

fracture occurs when the tensile stress at the crack tip reaches a critical value to propagate already existing micro-cracks. Carbides and non-metallic inclusions are believed to be the main sources of crack nucleation. The critical stress to propagate the pre-existing cracks hardly varies with temperature and, in this case, cleavage fracture strength only depends on the size of the pre-existing micro-cracks. In upper bainitic steel, carbide particles are abundant in the microstructure and cracks can easily be nucleated at the carbide particles. The independence of the cleavage fracture strength of alloy 'S' on temperature implies that the cleavage fracture of this steel occurs by the propagation of pre-existing micro-cracks.

3.2.2. Observation of micro-cracks

Fig. 7 shows the microstructural states just before the final cleavage fracture occurred in the double-notched bend specimens. Micro-cracks arrested at the ferrite lath boundaries, as shown in Fig. 7, were frequently observed

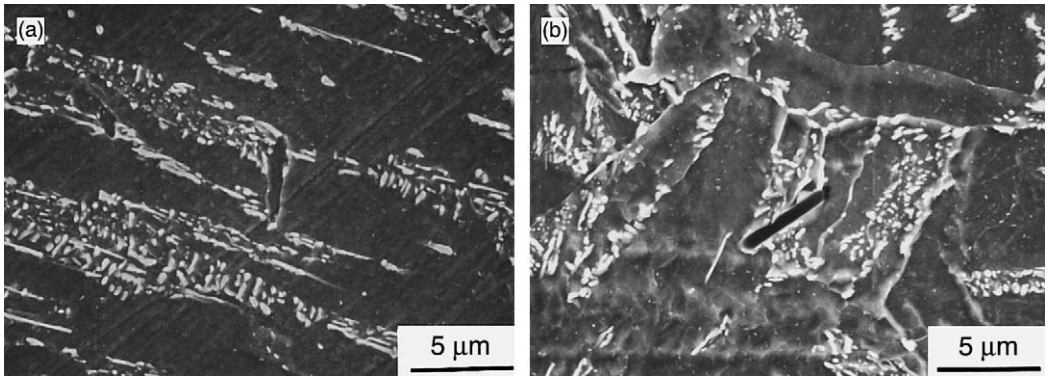

Fig. 7. Inter-lath cleavage nuclei observed in the higher carbon alloys in: (a) alloy 'S' [28]; (b) alloy 'A'.

in the cementite-crowded regions. The fracture of rod-like carbides or the de-cohesion of the carbide–ferrite interface has previously been reported in the ductile fracture of these alloys [28]. The easy formation of micro-cracks and their propagation in the cementite-crowded region at the initial stages of loading is feasible. The final cleavage fracture is believed to occur when the critical tensile stress at the crack tip of these inter-lath micro-cracks reaches a critical value.

3.2.3. Cleavage fracture strength of Mn–Ni–Mo alloys

The cleavage fracture strengths of the Mn–Ni–Mo alloys measured at −196 °C by the four-point bend test are given in Table 4 and are plotted as a function of the cementite volume fraction in Fig. 8. Fig. 8 shows that the cleavage fracture strength increases with decreasing cementite volume fraction of the alloys. The transition of the fracture mode from ductile to brittle occurs when the cleavage fracture stress becomes lower than the constrained flow stress of the alloy. The DBTT of an alloy will shift to lower temperatures, if either the cleavage fracture stress is increased or the flow stress is decreased. In the experimental alloys, used in this study, the yield stress was controlled at more or less a similar level, as shown in Tables 4 and 5. The decrease in the DBTT with the reduction in the cementite volume fraction ([28], Table 5) can be explained by the increase in the cleavage fracture strength of the alloy.

Table 4
Cleavage fracture strength of the tested alloys

Alloy	Yield strength at −196 °C (MPa)	Cleavage strength at −196 °C (MPa)
S	893	1674 (±45)
A	883	1691 (±60)
B	862	1862 (±78)
C	869	1903 (±96)
D	875	2004 (±88)

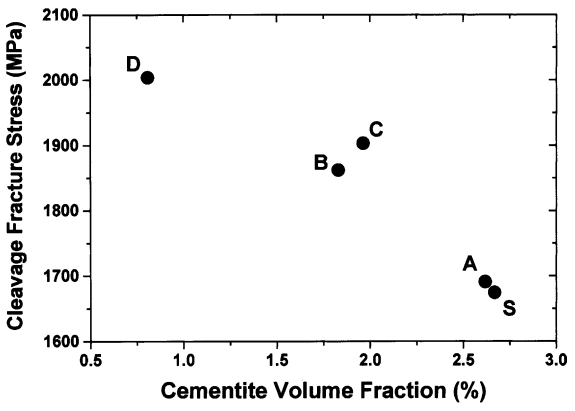

Fig. 8. The relationship between the cleavage fracture strengths and the calculated equilibrium volume fraction of cementite.

Table 5
Tensile and Charpy impact properties of the tested Mn–Ni–Mo alloys

Alloy	Tensile properties (MPa) at RT		Impact properties	
	YS	TS	USE (J)	DBTT (°C)
S	462	601	272	+8
A	451	586	227	−24
B	463	591	318	+3
C	468	582	241	−37
D	479	603	218	−29

3.2.4. Micro-mechanism of cleavage fracture in Mn–Ni–Mo bainitic steel

When cleavage fracture occurs by the propagation of pre-existing micro-cracks, the cleavage strength can be interpreted by the modified Griffith relationship. In this model, the size of the pre-existing micro-cracks determines the cleavage strength of the materials. In general, two types of Griffith relationships are considered in relation to the actual shape of defects. The defects formed by the fracture of spherical type carbides are treated as 'penny-shaped' ones (Eq. (1a)). The Griffith equation for the 'through-thickness' type is employed for defects with a much larger depth than the width (Eq. (1b)):

$$\sigma_{cf} = \left(\frac{\pi E \gamma_{eff}}{(1-\nu^2)a}\right)^{1/2}, \tag{1a}$$

$$\sigma_{cf} = \left(\frac{4E\gamma_{eff}}{\pi(1-\nu^2)a}\right)^{1/2}, \tag{1b}$$

where E is Young's modulus, γ_{eff} the effective surface energy, ν the Poisson's ratio, and a is the size of the defect.

In cases of mild steel, fracture of the inter-granular cementite film forms the 'through-thickness' type crack. In cases of upper bainitic steels, the shape of the defect formed by the fracture of rod-like cementite or the inter-lath cementite-crowded layer will be similar to a 'penny-shaped' one, since these microstructural units have spherical or elliptical cross sections. In Fig. 9, the cleavage fracture strengths of the upper bainitic Mn–Ni–Mo steels are related to the 95th percentile width of the cementite-crowded inter-lath layers via the Griffith equation. An effective surface energy of 12.4 J/m^2 was obtained from the Griffith plot, which is a reasonable value and within the range of the reported values of 7–14 J/m^2 for various types of steel [13,14].

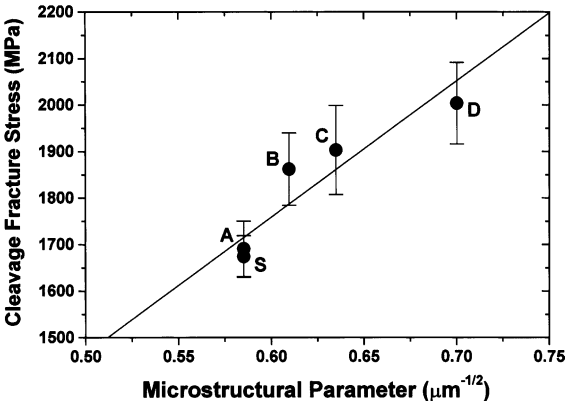

Fig. 9. The Griffith relation between the measured cleavage fracture strengths and the 95th percentile width of the inter-lath layers.

4. Discussion

Previous studies on the cleavage fracture of low carbon bainitic steels generally agree that the cleavage fracture of this type of steels occurs by the propagation of pre-existing micro-cracks. However, the authors do not agree with the microstructural units that control the cleavage resistance of the bainitic microstructure.

Brozzo et al. [22] investigated the relationship between the microstructure and the cleavage resistance in low carbon 2Mn–3Cr bainitic steels and concluded that the critical stage of the cleavage fracture process is the propagation of a Griffith crack from one bainitic packet to an adjacent one. Roberts [23], Ohmori et al. [24] and Kotilainen [25] all agreed that the cleavage facet size is directly related to the packet size even though they are not identical. These results all show that the packet size is the microstructural parameter that governs the cleavage fracture in lath microstructural steels.

On the other hand, Bowen et al. [14] reported that the carbide size distribution is the most important single microstructural feature that controls the cleavage fracture of a wide range of microstructures in A533B pressure vessel steel. However, the linear relationship between the cleavage strength and the square root of the coarsest carbide was obtained only when the carbide size was 340 nm or larger. Holzmann et al. [15] investigated the influence of tempering on the cleavage fracture of bainitic 2.25Cr–1Mo steel, and based on the observation that the cleavage strength decreased with increasing Hollomon–Jaffe [29] tempering parameters, they denied the dependence of the cleavage strength on the bainite packet size. Wallin et al. [16] and Saario et al. [17] also suggested the carbide size as a microstructural unit controlling the cleavage fracture in bainitic steel.

Curry [30,31] measured the cleavage fracture strength of SA508 cl.2 steel and claimed that the measured fracture strength values did not correspond to either the carbide particle size, the lath width or the packet sizes of the steel. He observed similar microstructural dependences of the yield and fracture stresses and suggested the involvement of some dislocation mechanisms such as those proposed by Cottrell [5] in the micro-mechanism of cleavage fracture.

In this study, the development of micro-cracks at the cementite-crowded regions in the upper bainitic microstructure was observed (Fig. 7). The 95th percentile size of these micro-cracks was 2–3 μm, which depends on the alloy carbon content and is of the order of the bainite lath width. A modified Griffith plot of the cleavage fracture strength against the inverse square root of the width of cementite-crowded region shows a fairly good linear relationship with an effective surface energy of 12.5 J/m^2, which is in good agreement with the reported value of 14 J/m^2 in ferrite [13]. The presence of finely dispersed M_2C type carbides may reduce the effective surface energy of the tempered bainitic Mn–Ni–Mo steels compared to that of the ferrite. The reported cleavage fracture strength of bainitic steels has ranged from 1500 to 2500 MPa [14,15,18,30,31]. These values, assuming 'penny-shaped' Griffith cracks and the effective surface energy of 12.5 J/m^2 obtained in this work, are equivalent to the Griffith crack length of 3.8–1.4 μm, which is the order of the bainite lath width. However, the effectiveness of the small angle lath boundaries in arresting running cracks has often been questioned. In addition, based on the observation that the cleavage facet size corresponds well to the packet size of the alloys, the idea that a micro-crack across a lath could be a precursor to fracture is normally dismissed.

In contrast to the martensitic or lower bainitic lath, the upper bainite structure contains inter-lath cementite-crowded areas, as shown in Fig. 3. The width of this cementite-crowded region is of the same order of the bainite lath width but decreases with increasing alloy carbon content. The crack arresting abilities of these inter-lath cementite-crowded regions will be much lower than the ferrite lath. For example, cracks initiated by the cracking of rod type carbide, may easily propagate through these cementite-crowded areas but may be arrested at the more ductile ferrite lath boundaries. The blunting of these micro-crack tips at the ferrite lath boundaries can be seen in Fig. 7. Such micro-cracks were frequently observed in the cementite-crowded areas close to the unbroken notches. When the tensile stress at the crack tip of a micro-crack reaches a critical value, a micro-crack propagates catastrophically through neighboring laths, resulting in cleavage fracture of the specimen. The orientation of the propagating crack would vary only slightly until it meets the packet boundaries because of the low angle characteristics of the lath boundaries. The cleavage facet size will well correspond to the packet size of the bainite because no significant

deflection in the fracture path will occur between the cementite-crowded inter-lath area and the adjacent ferrite lath.

5. Conclusions

The effects of alloy carbon content and microstructure on the cleavage fracture of low carbon bainitic Mn–Ni–Mo alloys were investigated. The following conclusions were made:

1. The DBTT and cleavage fracture strength of the alloys are strongly affected by the volume fraction of cementite. The reduction in the volume fraction of cementite resulted in a decrease in the width of the cementite-crowded inter-lath areas. The individual carbide particle size did not vary with the cementite volume fraction of the alloys.
2. The cleavage strength of the reference alloy 'S' was not dependent on the testing temperature, which suggests that cleavage fracture occurs by the propagation of micro-cracks when the tensile stress at the crack tip of the micro-cracks reaches a critical value.
3. Micro-cracks were frequently observed in the cementite-crowded areas close to the unfractured notches, and the size of the inter-lath cementite-crowded areas is proposed as the microstructural unit that controls the cleavage fracture of the upper bainitic microstructure.
4. A good correlation between the measured cleavage strengths and the width of the inter-lath cementite-crowded area was obtained via a modified Griffith relationship. The effective surface energy of 12.4 J/m^2 was obtained for the upper bainitic Mn–Ni–Mo alloys when the Griffith relationship for penny-shaped defects was applied.

Acknowledgements

This work was carried out as a part of the 'Reactor Pressure Boundary Materials Project' of the Korea Atomic Energy Research Institute under the Nuclear R&D Program supported by the Korea Ministry of Science and Technology. The authors wish to thank Professor Sunghak Lee of Pohang University of Science and Technology for his helpful discussions on the fracture behavior of alloys.

References

[1] A.A. Griffith, Phil. Trans. Roy. Soc. A 221 (1920) 163.
[2] C. Zener, Trans. ASM 40A (1948) 3.
[3] A.N. Stroh, Proc. Roy. Soc. A 223 (1954) 404.
[4] E. Smith, J.T. Barnby, Met. Sci. J. 1 (1967) 56.
[5] A.H. Cottrell, Trans. AIME 212 (1958) 192.
[6] P. Brozzo, M. Capurro, E. Stagno, Mater. Sci. Tech. 10 (1994) 334.
[7] E. Smith, in: Proceedings of the Conference on Physical Basis of Yield and Fracture, Institute of Physics and Physical Society, Oxford, 1966, p. 36.
[8] E.A. Almond, D.H. Timbres, J.D. Embury, in: P.L. Pratt (Ed.), Proceedings of the Second International Conference on Fracture, Chapman and Hall, London, 1969, p. 253.
[9] N.J. Petch, Acta Metall. 7 (1986) 36.
[10] C.J. McMahon, M. Cohen, Acta Metall. 13 (1965) 591.
[11] J.A. Hendrickson, D.S. Wood, D.S. Clarke, Trans. ASM 50 (1958) 656.
[12] J.F. Knott, J. Iron Steel Inst. 204 (1966) 104.
[13] D.A. Curry, J.F. Knott, Met. Sci. 12 (1978) 511.
[14] P. Bowen, S.G. Druce, J.F. Knott, Acta Metall. 34 (1986) 1121.
[15] M. Holtzmann, B. Vlach, J. Man, J. Krejčí, Steel Res. 6 (1995) 66.
[16] K. Wallin, T. Saario, K. Törrönen, Met. Sci. 18 (1984) 13.
[17] T. Saario, K. Wallin, K. Törrönen, J. Eng. Mater. Tech. 106 (1984) 173.
[18] L. Válka, M. Holzmann, I. Dlouhý, Mater. Sci. Eng. A 234–236 (1997) 723.
[19] J.T.H. Tweed, J.F. Knott, Met. Sci. 17 (1983) 45.
[20] D.E. McRobie, J.F. Knott, Mater. Sci. Tech. 1 (1985) 357.
[21] G.T. Hahn, B.L. Averbach, W.S. Owen, M.Cohen, in: B.L. Averbach, D.K. Felbeck, G.T. Hahn, D.A. Thomas (Eds.), in: Proceedings of Swampscott Conference on Fracture, Wiley, New York, 1959, p. 91.
[22] P. Brozzo, G. Buzzichelli, A. Manscanzoni, M. Mirabile, Met. Sci. 11 (1977) 123.
[23] M.J. Roberts, Metall. Trans. 1 (1970) 3287.
[24] Y. Ohmori, H. Ohtani, T. Kunitake, Met. Sci. 8 (1974) 357.
[25] H. Kotilainen, in: The Micromechanisms of Cleavage Fracture and Their Relationship to Fracture Toughness in a Bainitic Low Alloy Steels, PhD thesis, Technical Research Centre of Finland, Espoo, 1980.
[26] J.R. Griffiths, D.R.J. Owen, J. Mech. Phys. Solids 19 (1971) 419.
[27] B.-J. Lee, H.-D. Kim, J.-H. Hong, Metall. Mater. Trans. 29A (1998) 1441.
[28] Y.-R. Im, Y.J. Oh, B.-J. Lee, J.H. Hong, H.-C. Lee, J. Nucl. Mater. 297 (2001) 138.
[29] J.H. Hollomon, L.D. Jaffe, Trans. AIME 162 (1945) 223.
[30] D.A. Curry, Met. Sci. 16 (1982) 435.
[31] D.A. Curry, Met. Sci. 18 (1984) 67.